

Image-Based Malware Classification Using QR and Aztec Codes

Atharva Khadilkar* Mark Stamp*†

December 12, 2024

Abstract

In recent years, the use of image-based techniques for malware detection has gained prominence, with numerous studies demonstrating the efficacy of deep learning approaches such as Convolutional Neural Networks (CNN) in classifying images derived from executable files. In this paper, we consider an innovative method that relies on an image conversion process that consists of transforming features extracted from executable files into QR and Aztec codes. These codes capture structural patterns in a format that may enhance the learning capabilities of CNNs. We design and implement CNN architectures tailored to the unique properties of these codes and apply them to a comprehensive analysis involving two extensive malware datasets, both of which include a significant corpus of benign samples. Our results yield a split decision, with CNNs trained on QR and Aztec codes outperforming the state of the art on one of the datasets, but underperforming more typical techniques on the other dataset. These results indicate that the use of QR and Aztec codes as a form of feature engineering holds considerable promise in the malware domain, and that additional research is needed to better understand the relative strengths and weaknesses of such an approach.

1 Introduction

In the current digital age, cybersecurity threats have become increasingly sophisticated, one example of which is obfuscated malware. Obfuscated malware is malware that is “disguised” so that it is difficult to detect using conventional methods. Traditional antivirus systems rely on signature-based detection, which struggles to identify obfuscated malware [3].

*Department of Computer Science, San Jose State University

†mark.stamp@sjsu.edu

Malware classification is the process of categorizing various types of malware into distinct groups based on their behavior, characteristics, or potential impact. The conventional approach to malware classification is reliant on signature based and heuristic methods. In the malware context, signatures typically consist of known patterns that appear in the code, whereas heuristic analysis usually attempts to focus on behavioral patterns. These techniques struggle with the obfuscation strategies employed in modern malware, often leading to false positives or negatives.

Traditional machine learning (ML) methods have been used for enhancing malware classification offering an alternative to conventional signature based approaches [33]. A variety of traditional methods are commonly employed, including logistic regression, Support Vector Machine (SVM), and Random Forests. ML techniques significantly improves the detection of novel malware strain, as ML does not solely rely on pre-existing signatures. However, such ML methods can be challenged by sophisticated obfuscation techniques. A recent trend in malware detection consists of converting executable files to images and using sophisticated image analysis techniques for classification. This approach is promising and has shown improved results over traditional ML techniques. However, the process used to convert executables to images can have a large impact on the success of such image-based analysis techniques.

Building on traditional ML methods for malware classification, we propose to use QR and Aztec codes as image representations of data, combined with advanced image classification techniques. By leveraging the unique patterns within these images, our method aims to improve on image-based analysis of obfuscated malware. We find that our approach offers an improvement over traditional features and also improves on typical image-generation techniques for the detection of complex malware variants.

The remainder of this paper is organized as follows. Section 2 discusses relevant previous work, including traditional and image-based techniques for malware detection and classification. Section 3 introduces the datasets utilized in this study, detailing their composition, source, and the methodology employed for their collection and preparation. Section 4 outlines the libraries and platforms used in our experiments. Following this, Section 5 covers the techniques and methodologies employed, along with a discussion of the implementation of these methods. Section 6 includes the results of our experiments and compares our results to previous related work. Section 7 concludes the paper, summarizing our key findings and discussing potential avenues for future research.

2 Selected Related Work

This section explores selected prior research in the realm of malware detection, particularly focusing on approaches that use image representation for identifying malware. Additionally, we explore studies related to the detection of obfuscated

malware, emphasizing techniques that utilize memory dumps. These topics represent significant advances in malware detection.

2.1 Obfuscated Malware

Obfuscated malware techniques complicate the detection process by disguising the malicious code, making it challenging for traditional antivirus solutions to identify threats effectively. Techniques such as polymorphism and metamorphism are frequently employed, allowing malware to alter its code with each replication, thereby evading signature-based detection systems. The research in [38] detail these methods, noting their sophistication and the difficulty they pose to detection efforts. Similarly, [6] discuss the theoretical underpinnings of code obfuscation, pointing out the effectiveness of such techniques in protecting malware from analysis. These approaches highlight the continuous arms race between cybersecurity professionals and attackers, underscoring the need for advanced detection methods capable of penetrating these obfuscations.

The CIC-MalMem-2022 dataset [8] contains features extracted from obfuscated malware samples. Studies focusing on binary classification using the CIC-MalMem-2022 dataset, such as [13, 17], have applied various ML techniques, achieving up to 0.9997 accuracy with learning methods such as Decision Trees and SVC. Additionally the research in [17] employs feature engineering and tree-based techniques such as XGBoost and CatBoost, achieving a 1.00 accuracy in binary classification with a Random Forest Classifier. This demonstrates the effectiveness of combining advanced methods and feature engineering in improving malware detection.

2.2 Behavioral Analysis of Malware

Malware behavior analysis techniques focus on observing the actions of malware within a system, offering insights beyond those that static analysis can provide. This dynamic approach, as considered in [7] and [31], for example, involves monitoring the execution patterns and network behaviors of malware to classify and understand its nature. Such techniques are critical in identifying new variants of malware by examining their behavior patterns, potentially offering more adaptive and robust mechanism for threat detection. The effectiveness of these methods lies in their ability to provide a detailed view of malware operations, contributing to the development of more precise and effective cybersecurity measures.

2.3 Image Representations

The conversion of malware binaries into visual images for analysis has recently shown great promise. The papers [19, 20, 26] explore the potential of such techniques, which leverages the visual patterns that emerge from the binary code of malware when represented as images. These methods allow for the application of

advanced image processing techniques to identify distinctive features associated with malicious software. The advantage of image representation lies in its ability to reveal patterns that are not easily discernible through traditional binary analysis, providing an alternative avenue for the detection and classification of malware.

The use of Convolutional Neural Networks (CNNs) for classifying malware based on image representations showcases the application of deep learning in cybersecurity. For example, the research in [16, 19] demonstrates the effectiveness of CNNs in analyzing the visual patterns of malware images to accurately classify different types of malware. These studies highlight the ability of CNNs to learn and identify complex patterns within images, facilitating a highly effective classification system. Another strength of this approach lies in its capacity to process and analyze large datasets of malware images, thus offering a scalable and efficient solution for the identification of malware.

2.4 Advanced CNN Architectures

The convergence of Convolutional Neural Networks and pre-trained models has significantly advanced malware classification, leveraging deep learning for cybersecurity. The studies in [1, 23], for example, highlight the effectiveness of pre-trained CNN models. Examples of such pre-trained models include VGG16, ResNet-50, and DenseNet-201. Additionally, these works delve into the challenges associated with feature extraction, feature engineering, computational demands, dataset imbalances, and so on. These are issues often encountered when learning techniques are used in the malware domain.

Further innovations include ensemble and transfer learning approaches to enhance accuracy and efficiency in malware-related tasks. For instance, in [15, 23] the application of fine-tuned CNN-based transfer learning models on transformed 2D images of malware binaries demonstrated exceptional detection accuracies, outperforming conventional methods. More generally, these approaches signify a shift towards utilizing deep learning models to deal with the challenges of evolving cybersecurity threats.

2.5 Memory Dump Analysis

Memory dump analysis for malware classification involves examining snapshots of system memory to detect potentially malicious behavior. This technique, as discussed in [10, 11, 12] provides valuable insights into the runtime behavior of malware. Memory dump analysis is particularly effective in identifying malware that employs evasion techniques, as it allows for the examination of the system state at the time of execution, at which point most obfuscation techniques have run their course. This approach enhances the capability to classify and analyze complex malware, underscoring its importance in the comprehensive examination of cyber threats.

2.6 QR Codes

Quick Response (QR) codes are 2D bar codes that can encode virtually any type of data, and are easily readable by devices such as smartphone cameras. A QR code can encode up to 7089 digits, 4296 alphanumeric characters, 2953 bytes, or 1817 Kanji characters, although these values may be reduced, depending on the level of error correction that is applied [28].

For our purposes, QR codes provide a basis for applying image-based learning techniques to virtually any type of data. The research in [36] exemplifies this by evaluating various pre-trained CNN models, including AlexNet and MobileNetv2, to accurately identify the source printer of QR codes. This example highlights the potential for merging QR code versatility with CNN image-based learning capabilities, offering a novel pathway for data classification that has the potential to significantly enhance information security. The paper [29] explores another approach which uses CNNs to classify malware based on QR code representations of data.

2.7 Aztec Codes

Aztec codes are similar to QR codes, but they can be more space-efficient for a given amount of data. An Aztec code can encode a maximum of 3832 numeric digits, 3067 alphabetic characters, or 1914 bytes of data [4]. As far as the authors are aware, Aztec codes have not been previously studied in the context of malware analysis, or in conjunction with image-based learning techniques.

3 Datasets

In this section, we provide an overview of the datasets used in this research. We consider two distinct datasets, one of which consists of dynamic features extracted from obfuscated malware, while the other consists of static features extracted from typical malware.

3.1 CIC-MalMem-2022

The paper [9] focuses on improving malware detection, specifically targeting obfuscated malware. The study uses the VolMemLyzer tool, a memory feature extractor, to better identify hidden and obfuscated malware. A significant contribution is the creation of the MalMemAnalysis-2022 dataset, which includes over 2500 malware samples in the broad categories of spyware, ransomware, and Trojan horse, as well as a representative benign set. The authors employ a stacked ensemble ML model for detection, achieving high accuracy and F1-score for the binary classification problem.

Based on the work in [9], the CIC-MalMem-2022 dataset was published [8]. This dataset includes features extracted using a memory dump operation in debug mode. This method is specifically designed to prevent the dumping process itself from being recorded in the memory dumps, which ensures that only the relevant data is captured. The dataset consists of a total of 58,596 samples extracted from 2916 malware executables and 2916 benign executables, with a minimum of 100 and a maximum of 200 samples per executable. The malware executables are from three major categories, namely, ransomware, spyware, and Trojan horse.

From this dataset, we use 6000 samples chosen randomly for each of the three malware categories, and 6000 benign samples. These 24,000 samples are the basis for training and testing our multiclass models using the learning techniques discussed in Section 5, below. The distribution of samples from the CIC-MalMem-2022 dataset is given in Figure 1.

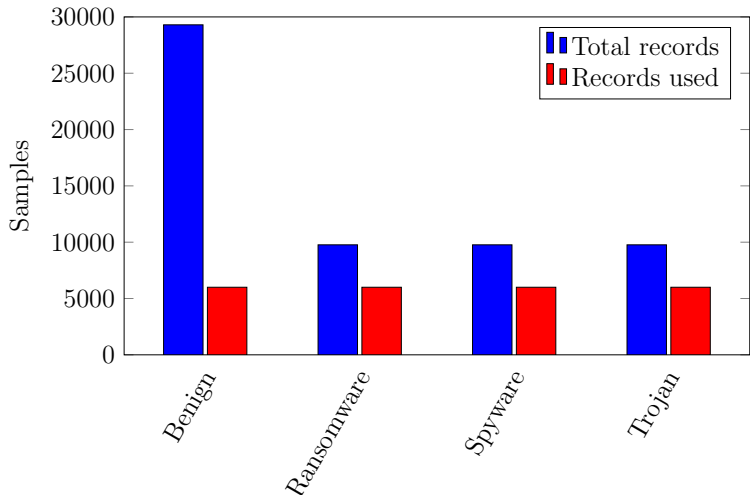


Figure 1: CIC-MalMem-2022 class distribution

3.2 BODMAS

The BODMAS dataset [37] is a collaborative effort between Blue Hexagon and the University of Illinois at Urbana-Champaign (UIUC), and it represents a valuable resource for the cybersecurity research community. This dataset consists of 57,293 malware samples and 77,142 benign samples, collected between August 2019 and September 2020. This substantial collection, which includes samples spanning 581 malware families, is notable for including date of origin of each sample, thus providing a resource for temporal-based analysis and classification of malware.

The feature vectors for each of the malware sample was extracted using the LIEF project, similar to the EMBER [2] dataset. Executable file formats share

common features including symbols, relocations, and entry-point. Each malware sample has a feature vector of dimension 2384 and associated metadata. This metadata includes details such as timestamp, label (malware or benign), and the specific malware family of the sample. The feature vectors consist of features parsed from the PE file, including the SHA256 hash of the file, header characteristics, entry points, entropy, and various histograms [2].

Since the BODMAS dataset consists of approximately 58,000 malware samples from 581 malware families, we selected a handful of the most frequently occurring families for our analysis, along with a subset of benign samples. The distributions of the benign class and the top 10 families in the BODMAS dataset are shown using Figure 2. We have selected 13,324 samples consisting of the top three malware families, namely, *Sfone*, *Wacatac*, and *Upatre*, along with 5200 benign samples for a total of 18,524 samples. Similar to the CIC-MalMem-2022 dataset, we apply the learning techniques discussed in Section 5, below.

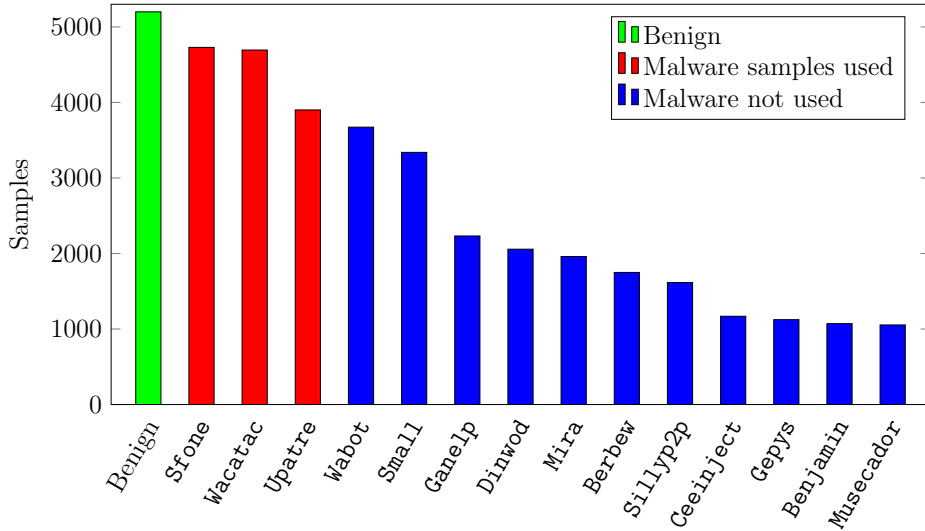


Figure 2: Benign and BODMAS class distribution

4 Implementation

This section provides a comprehensive overview of the software and libraries used in our research. Here, we introduce each chosen platform and library, specifying its role, benefits, and the reason for its selection.

4.1 Machine Learning Tools

The implementation of our research involves data exploration of two datasets. Along with this, we also explore feature selection and model training. The

models vary from classical ML to pre-trained DL models. These models vary greatly in the amount of complexity, and they required different libraries to be used. Due to the availability of necessary packages, Python 3.9 was used throughout our experiments. Specifically, the following Python libraries were used.

- **scikit-learn** — The Python library `scikit-learn` is designed for machine learning [30]. It offers tools for data preprocessing, model building, and evaluation. It also includes algorithms for both supervised and unsupervised learning such as regression, decision trees, clustering, and Support Vector Machines. `scikit-learn` is designed to work with NumPy and SciPy. We use `scikit-learn` for some of the classical ML algorithms and for feature selection. `scikit-learn` was also used to calculate our performance metrics (accuracy, F1-score) for our classic ML models.
- **TensorFlow** — TensorFlow is an open-source library for numerical computation and ML [35]. It provides a flexible platform for building and deploying a wide range of ML models. TensorFlow supports deep learning algorithms along with many traditional ML models. The library includes tools for data processing, model creation, training, and inference. TensorFlow was used to form our generated QR and Aztec codes into image datasets. It was also used to construct and train our Convolutional Neural Networks.

4.2 Utilities

The following packages and libraries were also used in our research. These tools are not directly used for ML, but they are necessary to prepare the data for our models.

- **Pandas** — Pandas is a Python library for data manipulation and analysis [24]. It provides data structures including DataFrame and Series for handling tabular data. Pandas is equipped with tools for reading and writing data between in-memory data structures and different file formats. We use this library for the manipulation and preprocessing of our data.
- **NumPy** — NumPy is a fundamental package for scientific computing in Python [21]. It provides support for large arrays and matrices, along with a collection of mathematical functions to operate on these arrays. NumPy was used along with Pandas to enabling efficient processing of the data.
- **Qrcode** — The Python library `qrcode` is designed to generate QR codes [27]. It allows for the creation and customization of QR codes that can encode a wide range of data types, including URLs, text, or numerical information. This library provides a simple interface for QR code generation, offering flexibility in terms of size, border, and error correction levels. Of course, we employ this library to create QR representations of our data.
- **AztecCode** — AztecCode from `aztec_code_generator` is a Python library designed for creating Aztec codes, a type of 2D barcode that can store a

significant amount of data within a small space [5]. Similar to QR codes, but with significant differences in design and capacity, Aztec codes are used in various applications, especially where space and readability are critical. The `aztec_code_generator` library provides functionality to generate and customize these codes, including setting size, encoding data, and adjusting error correction levels. This library was used to generate the Aztec code representation of the data used in our experiments.

- **Operating System** — The standard Python library `OS` provides a way to use operating system-dependent functionality [22]. It includes functions for interacting with the file system, such as creating, listing, and deleting files and directories. We primarily use `OS` for data organization during the image generation process.
- **Pillow** — The `Image` module from Pillow, the Python Imaging Library, supports opening, manipulating, and saving many different image file formats [25]. It provides a wide array of image processing capabilities, including image transformations (e.g., rotation and scaling), filtering, enhancement, and so on. We use Pillow for post processing on our generated QR and Aztec codes.

4.3 Development Platforms

Google Colab was an essential part of our model training. Here, we provide some details on our use of Colab and also our local computer setup.

- **Google Colab** — Throughout our experiments, the Google Colab platform was used extensively for data processing, data conversion, and training learning models. The platform provides access to most of the libraries discussed above, including TensorFlow and `scikit-learn`. The platform offers multiple environment runtimes with the option of choosing GPUs. Using GPU hardware acceleration reduced the training times for our CNNs by a factor of about four, as compared to the CPU hardware accelerators.
- **Local Computer** — In addition to Google Colab, we used a local desktop setup to execute some of our experiments. The local setup served multiple purposes, including visualization and data exploration, as well as for data preprocessing and cleaning. We also generated the QR and Aztec code images using this local machine. The operations were performed locally using Visual Studio Code by creating a Python 3.9 virtual environment. The specifications of the local machine are given in Table 1.

5 Methodology

In this section we describe the machine learning models and methods used to generate our experimental results. This section introduces each learning method and provides reasons why these methods were used in the context of this research.

Table 1: Local machine

System	Specification
CPU	AMD Ryzen 5600X
CPU clock rate	4.6 GHz
GPU	NVIDIA RTX 3080 (10GB)
CUDA core	8704
Cores	6
RAM	32GB
OS	MS Windows 10

5.1 Feature Selection

Considering the large number of features in our datasets, feature reduction is an important aspect to this research. For this purpose we consider the following feature selection methods.

SelectKBest from `scikit-learn` is a statistical method used to select features that have the most significant relationship with the output variable. This works by applying a chosen statistical test to each feature to determine its strength of association with the output variable. The K in **SelectKBest** refers to the number of features to select based, on their ranking. We selected features after normalizing using the standard scaler.

Statistical tests available in **SelectKBest** include the ANOVA F-test for continuous data and χ^2 for categorical data. We have used χ^2 for selecting our K best features. This method is effective in feature reduction, helping to improve model performance by eliminating irrelevant or redundant features. It is particularly useful in helping us reduce the number of features before converting the data into a QR or Aztec code, since these representation can only hold a limited number of bytes.

5.2 Machine Learning Models

In this section, we describe all of the ML models used in this research including the classical and deep learning models. We also mention why each model was chosen for this research.

5.2.1 Random Forest

The Random Forest classifier from `scikit-learn` is an ML algorithm for classification tasks. It operates by constructing multiple decision trees during the training phase and outputs the class that is the mode of the classes of the individual trees. This approach to combining multiple models to improve the overall result is an example of ensemble learning.

The Random Forest algorithm can handle both numerical and categorical data and is capable of dealing with large datasets efficiently. Additionally, it provides measures of feature importance, which can be used for feature selection. Random Forest is widely used across various fields for its robustness against overfitting, compared to a single decision tree, making it a popular choice for complex classification problems.

5.2.2 Support Vector Machine

Support Vector Machine (SVM) from `scikit-learn` is a supervised ML algorithm used for both classification and regression tasks, though it is primarily known for classification. The core principle of SVM is to find the hyperplane that best divides a dataset into classes. SVM is distinctive for its use of kernels, which transform the input data space into a higher dimensional space where it becomes easier to separate the data linearly. This makes SVM effective for complex datasets where the relationship between features may not be clear.

The performance of SVMs depend heavily on the selection of the kernel and the tuning of the hyperparameters, which can sometimes make it challenging to optimize. SVM is widely utilized in applications ranging from image classification to bioinformatics, due to its robustness and versatility.

Support Vector Classifier (SVC) is a generalization of SVM to the multiclass case. SVC works by finding multiple hyperplanes that best separate different classes with the maximum margin. This makes SVC particularly effective for complex classification problems where the decision boundary is not immediately obvious.

5.2.3 Multilayer Perceptron

The Multilayer Perceptron (MLP) classifier from `scikit-learn` is a basic type of artificial neural network that is used for classification and regression tasks. Unlike simpler linear models, MLP can model complex nonlinear relationships between inputs and outputs. An MLP includes at least three layers consisting of an input layer, one or more hidden layers, and an output layer. The nodes, or neurons, in each layer are fully connected to those in the next layer, and activation functions serve to introduce nonlinearity to the learning process [34].

Training an MLP involves adjusting the weights of the connections through a process known as backpropagation, which minimizes the difference between the actual and predicted outputs. MLP is particularly useful for problems where the relationship between input and output is not linearly separable. The performance of an MLP is influenced by various factors, including the number of hidden layers, the size of these layers, and the choice of activation function. MLPs are widely used in a variety of fields, including speech recognition and natural language processing.

5.2.4 Convolutional Neural Networks

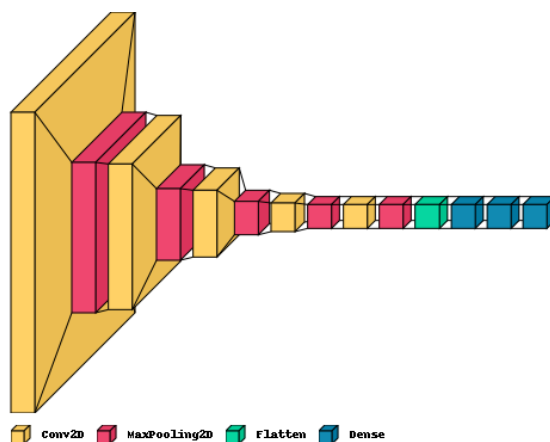
Convolutional Neural Networks (CNNs) are a basic class of deep neural networks, widely utilized in the field of computer vision. Developed with inspiration from the human visual cortex, CNNs excel at automatically and adaptively learning spatial hierarchies of features from image data. They consist of multiple layers, including convolutional layers that capture patterns such as edges and textures, pooling layers that reduce dimensionality and computational complexity, and fully connected layers that classify the images based on the features extracted by convolutional and pooling layers.

Our CNNs are implemented using the keras library, a high-level neural networks API that runs on top of TensorFlow [35]. Keras provides a user-friendly interface for building and training CNN models, offering a flexible and efficient way to design deep learning models with just a few lines of code.

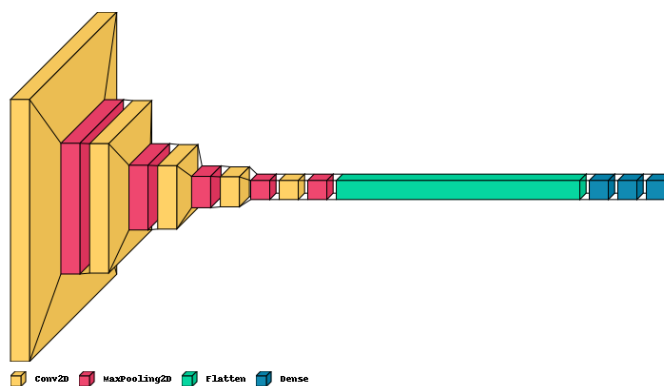
Due to the different features available with the two datasets we consider, we employ two distinct CNN architectures. Here, we describe both of these architectures in some detail.

- **CNN for CIC-MalMem-2022 dataset** — Our CNN architecture for the CIC-MalMem-2022 dataset has an input size of $128 \times 128 \times 1$ which is the size of the QR and Aztec codes generated from the dataset. The initial convolutional layer consists of 32 filters of size 3×3 , which yields an output of size $126 \times 126 \times 32$. There are four more convolutional layers which have output sizes of $61 \times 61 \times 64$, $28 \times 28 \times 128$, $12 \times 12 \times 256$, and $4 \times 4 \times 512$, respectively. Each convolutional layer is followed by a max pooling layer and the final output of all these layers is $2 \times 2 \times 512$. This is then flattened and forwarded to three dense layers for classification. Our CNN for the CIC-MalMem-2022 dataset is illustrated in Figure 3(a).
- **CNN for BODMAS dataset** — Our CNN for the BODMAS dataset has a similar structure as that for the CIC-MalMem-2022 dataset. However, for this CNN the input layer is $395 \times 395 \times 1$, since this is the size of our QR images generated from the BODMAS data. This slightly alters the remaining parts of the model.

The initial convolutional layer consists of 32 filters of size 3×3 , which yields an output of size $393 \times 393 \times 32$. There are four more convolutional layers which have output sizes of $194 \times 194 \times 64$, $95 \times 95 \times 128$, $45 \times 45 \times 256$, and $20 \times 20 \times 512$, respectively. Each convolutional layer is followed by a max pooling layer and the final output of all these layers is $10 \times 10 \times 512$. This is then flattened and forwarded to three dense layers for classification. The CNN architecture that we use for the BODMAS dataset is illustrated in Figure 3(b).



(a) Model for CIC-MalMem-2022 dataset



(b) Model for BODMAS dataset

Figure 3: CNN architectures

6 Experiments and Results

This section is split into two main parts, each describing the results for one of the two datasets that we consider. We summarize the overall results at the end of this section and we discuss our main findings.

6.1 CIC-MalMem-2022 Results

As discussed above, for the CIC-MalMem-2022 dataset, each sample consists of 55 features. We first consider feature analysis to understand the relative importance of features in the dataset.

For feature selection, we use SelectKBest from `scikit-learn`, with the χ^2 option. SelectKBest determines the top K features that have the highest χ^2 values with respect to the target variable. The χ^2 test measures the dependence

between stochastic variables, making this method suitable for determining the statistical significance of features. The top 10 features of highest importance in the CIC-MalMem-2022 dataset are listed in Table 2; a complete list of all 55 features is given in Table A.1 in Appendix A.

Table 2: Top 10 features for CIC-MalMem-2022 dataset

Rank	Feature name
1	<code>malfind.commitCharge</code>
2	<code>handles.nhandles</code>
3	<code>handles.nevent</code>
4	<code>handles.nsection</code>
5	<code>handles.nthread</code>
6	<code>dlllist.ndlls</code>
7	<code>handles.nfile</code>
8	<code>handles.nkey</code>
9	<code>handles.nmutant</code>
10	<code>handles.nsemaphore</code>

6.1.1 Classic Learning Techniques

In this section, we consider experiments involving Random Forest, SVC, and MLP classifiers. The following experiments were conducted using the entire set of 55 features. We also experimented with the reduced set of 10 features in Table 2, but the results are similar.

When trained on the entire set of 55 features with 1000 estimators, Random Forest achieves an accuracy of 0.7979. From the confusion matrix in Figure 4(a), we observe that all the benign examples were classified correctly; however the classifier had considerable difficulty distinguishing between the three malware categories. The F1-score for this classifier is 0.7980

When trained on the set of 55 features, SVC achieves an accuracy of 0.5343. The confusion matrix in Figure 4(b) further emphasizes the poor performance of this model. The F1-score achieved using this method is 0.4597 which is also much worse than the Random Forest.

When trained on the full 55 features, our MLP classifier achieves 0.5391 accuracy. The confusion matrix in Figure 4(c) shows that this MLP model tends to make different types of mistakes than the SVC. The F1-scores achieved by our MLP model is 0.4886, which is similar to that of the SVC.

Table 3 summarizes the accuracies and F1-scores for the Random Forest, SVC, and MLP classifiers, both with and without feature reduction. We observe that feature selection has little effect on the performance of these models.

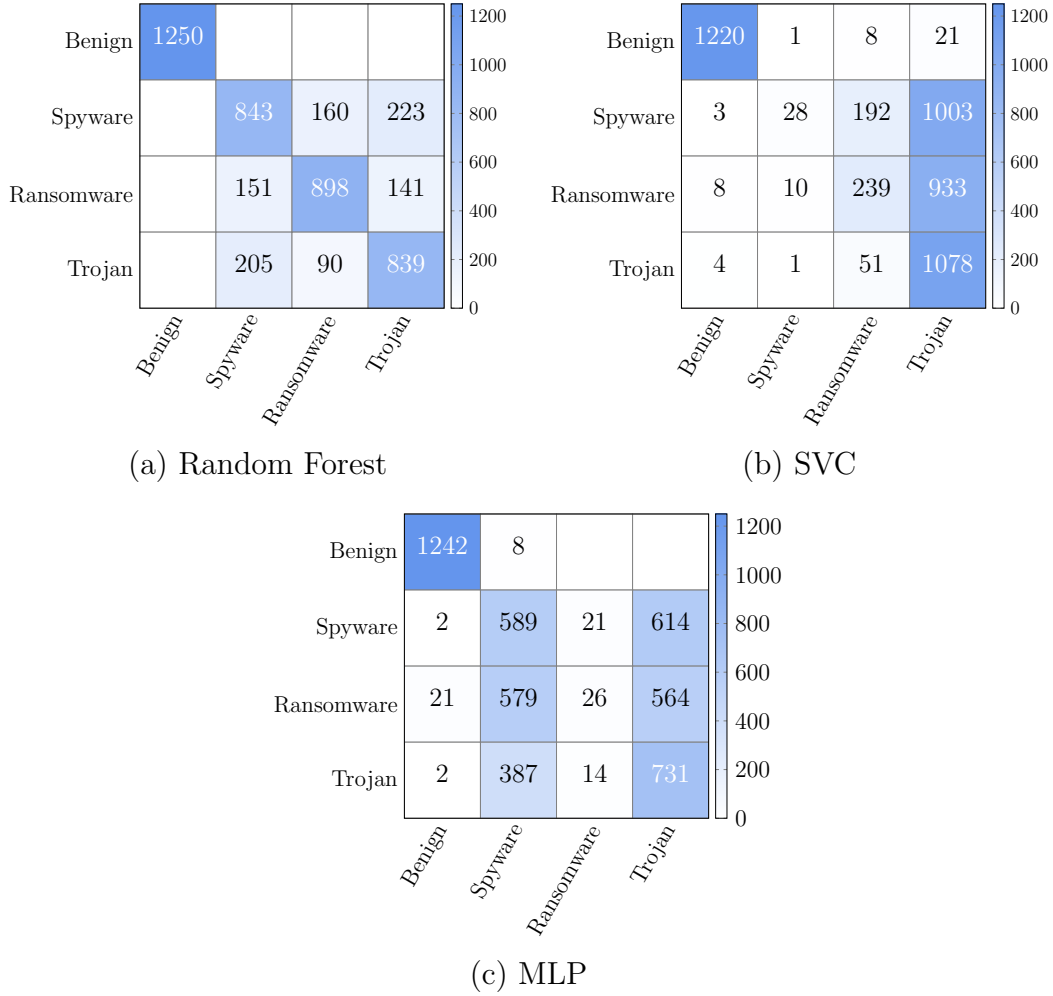


Figure 4: Confusion matrices for classic techniques (CIC-MalMem-2022)

Table 3: Accuracies and F1-scores (CIC-MalMem-2022 dataset)

Measure	Features	Random Forest	SVC	MLP
Accuracy	55	0.7979	0.5343	0.5391
	10	0.7689	0.5395	0.5483
F1-score	55	0.7980	0.4597	0.4886
	10	0.7690	0.4615	0.4710

6.1.2 QR Code Experiments

To create our QR representations for the CIC-MalMem-2022 dataset, the top 10 features were used. Figures 5(a) through (d) give examples of QR representations of benign, ransomware, spyware, and Trojan, respectively.



Figure 5: Examples of QR code representations (CIC-MalMem-2022)

The parameters used to generate the QR codes for this dataset are given in Table 4. The generated images were of size 175×175 pixels each. These were then resized to images of size 128×128 before being used as input to the CNN.

Table 4: QR parameters for CIC-MalMem-2022

Parameter	Value
version	1
error_correction	ERROR_CORRECT_L
box_size	5
border	1

We split the 24,000 samples 70:15:15 for train:validation:test. The train and validation split was used to train on the CNN model described in Section 5. The loss and accuracy graphs are shown in Figure 6. These graphs show that the model converged after two epochs, with no signs of overfitting. The test accuracy achieved for the CNN on the QR image representation was 0.9998 for this multiclass classification problem.

6.1.3 Aztec Code Experiments

To create the Aztec code representation, as for the QR codes, we use the top 10 features. Figures 7(a) through (d) give typical examples of Aztec code representations for the benign, ransomware, spyware, and Trojan classes, respectively.

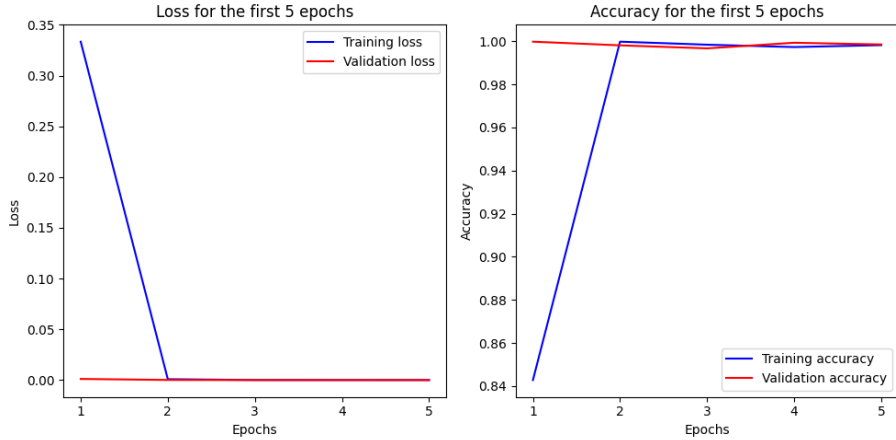


Figure 6: QR-CNN accuracy and loss graphs for CIC-MalMem-2022

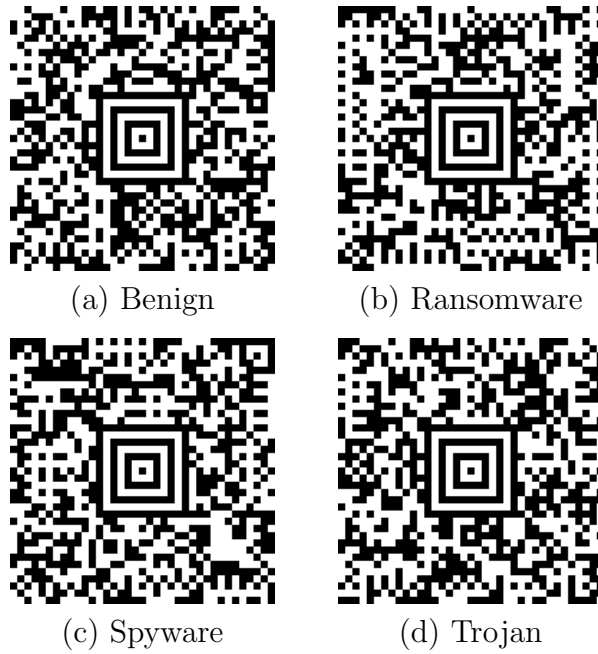


Figure 7: Examples of Aztec code representations (CIC-MalMem-2022)

The only parameter that we employ when generating our Aztec code representations is `module_size = 5`. The generated images are of size 175×175 pixels, and these were then resized to images of size 128×128 so as to be suitable as input to the CNN.

We split the samples 70:15:15 for train:validation:test. The train and validation split was used to train the CNN architecture described in Section 5. The loss and accuracy graphs for this model are shown in Figure 8. As with the QR-CNN results in Figure 6, the graphs in Figure 8 show that the model converges after two epochs, with no indication of overfitting.

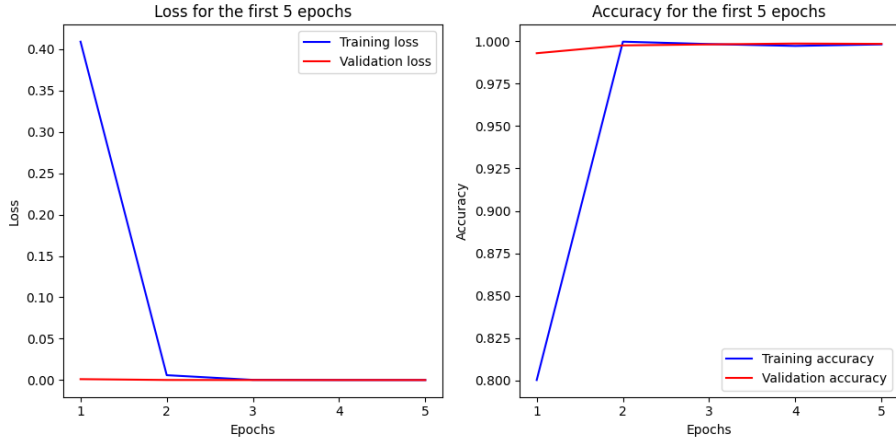


Figure 8: Aztec-CNN accuracy and loss graphs for CIC-MalMem-2022

The test accuracy achieved for the CNN on the QR image representation was 0.9986 for this multiclass classification problem. While this is marginally less than the accuracy achieved using the QR code representation, both represent nearly perfect classification.

6.2 BODMAS Results

In this section, we conduct analogous experiments as the previous section, but based on the BODMAS dataset, rather than the CIC-MalMem-2022 dataset. We first discuss feature selection before turning our attention to our experimental results.

6.2.1 Feature Selection

Recall that each BODMAS sample consists of a 2384 dimensional vector, which was extracted using the LIEF project. For the classic ML models, we experiment with the top 50 and the top 150 features. Similarly, our CNN models are trained on QR and Aztec images derived from the same top 50 and top 150 features.

Figure 9 shows the distribution of the top 150 features among the 2384 BODMAS features. This figure highlights the fact that most of the features are of little—if any—relevance for classification.

The feature selection for the BODMAS dataset was done by selecting the top 50 features using `SelectKBest` with ANOVA as the a statistical technique. The 10 most significant features for the BODMAS dataset are shown in Table 5.

6.2.2 Classic Learning Techniques

When trained on the set of 50 features with 1000 estimators, the Random Forest achieves an accuracy of 0.946. From the confusion matrix in Figure 10(a), we

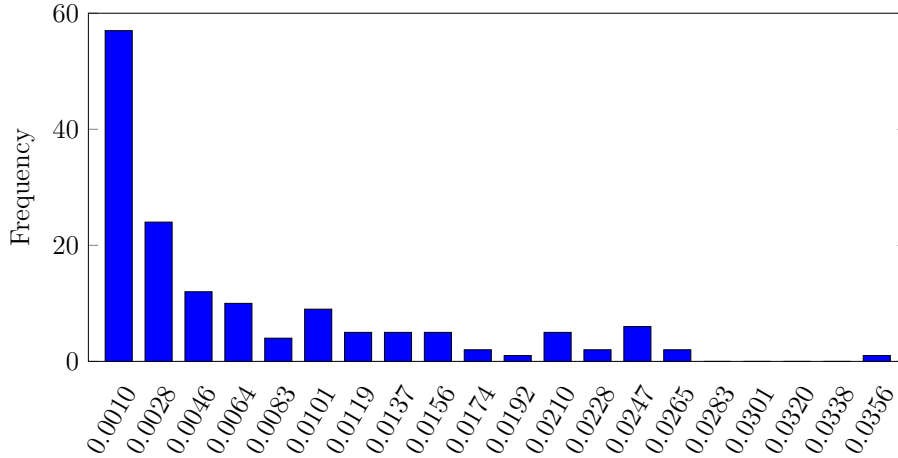


Figure 9: Feature importance distribution in BODMAS

Table 5: Top 10 features for BODMAS dataset

Rank	Feature number	Importance
1	584	0.036483
2	473	0.026751
3	1283	0.025871
4	137	0.024794
5	44	0.024691
6	506	0.024518
7	62	0.024090
8	38	0.024042
9	499	0.023880
10	27	0.022573

observe that almost all the benign examples are classified correctly, while the classifier has more difficulty with the three malware classes.

When trained on 50 features, SVC achieves an accuracy of 0.9190, while our MLP classifier achieves 0.9482 accuracy. The confusion matrices in Figures 10(b) and (c) show us that both of these classifiers more often misclassify **Sfone** as **Upatre**, as compared to any other misclassification.

6.2.3 QR Code Experiments

To generate QR representations of the data, the top 50 features were used. Figures 11(a) through (d) are examples of the benign, **Sfone**, **Upatre**, and **Wacatac** classes, respectively.

The parameters used to generate these QR are given in Table 6. The generated images are of size 395×395 pixels. These were resized to 128×128 images

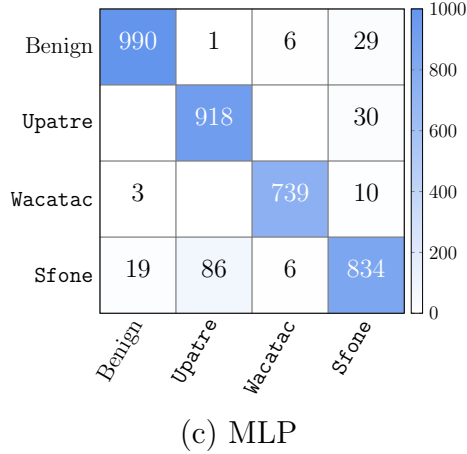
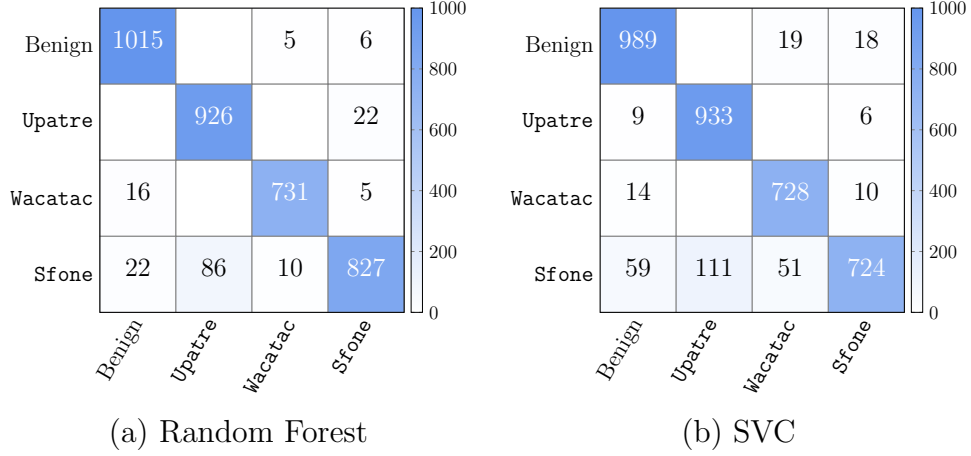


Figure 10: Confusion matrices for classic techniques (BODMAS dataset)

Table 6: QR parameters for BODMAS dataset

Parameter	Value
version	1
error_correction	ERROR_CORRECT_L
box_size	5
border	1

for use as input to our CNN.

To train our CNN model, the 18,524 samples were split 80:20 to train:test. The validation split was not done in this case due to the smaller number of samples available. The loss and accuracy graphs for this CNN model are shown in the following Figure 12, where we see some indications of overfitting.

The test accuracy achieved for the CNN on the QR image representation was 0.8271 for this multiclass problem. Note that this accuracy is less than we



Figure 11: Examples of QR code representations (BODMAS)

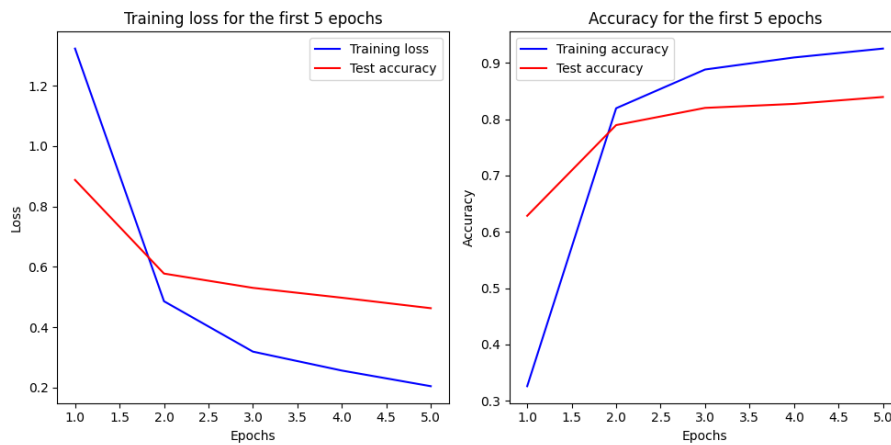


Figure 12: QR-CNN accuracy and loss graphs for BODMAS (50 features)

achieved with each of our three classic ML techniques.

We repeated this experiment using 150 features. The loss and accuracy graphs for this case are shown in Figure 13. In this case, there appears to be less overfitting, as compared to the model based on 50 features.

The test accuracy achieved for the CNN based on 150 features is 0.8971. This result improves significantly on the case where 50 features are considered, but it is still less than our best classic ML technique.

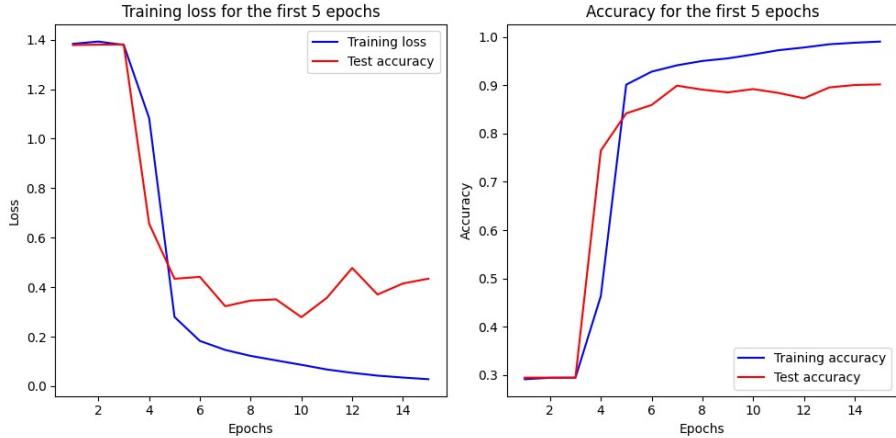


Figure 13: QR-CNN accuracy and loss graphs for BODMAS (150 features)

6.2.4 Aztec Code Experiments

For the Aztec code representations of the data, we follow the same procedure as was used for our QR code experiments, above. Specifically, we experiment using 50 features, then we repeat the entire set of experiments based on 150 features.

Figures 14(a) through (d) are representative examples of Aztec codes, based on 50 features, for the benign, *Sfone*, *Upatre*, and *Wacatac* classes, respectively. As above, the only parameter used for these Aztec codes was `module_size = 5`.

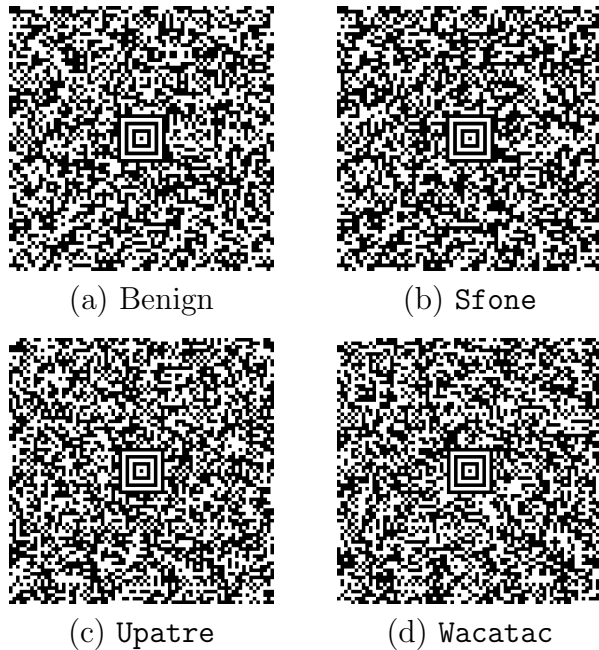


Figure 14: Examples of Aztec code representations (BODMAS)

The generated Aztec images are of size 375×375 pixels. These are directly used as input to our CNN architecture, which is described in Section 5. Note that no resizing is necessary. Also, when training, we use an 80:20 split for training and testing. As with the QR code case, a validation split was not used in this case.

The loss and accuracy graphs for this case are shown in Figure 15. It is clear that the model starts overfitting from epoch three. The test accuracy achieved for the CNN on the Aztec image representation was 0.7821 for this multiclass problem.

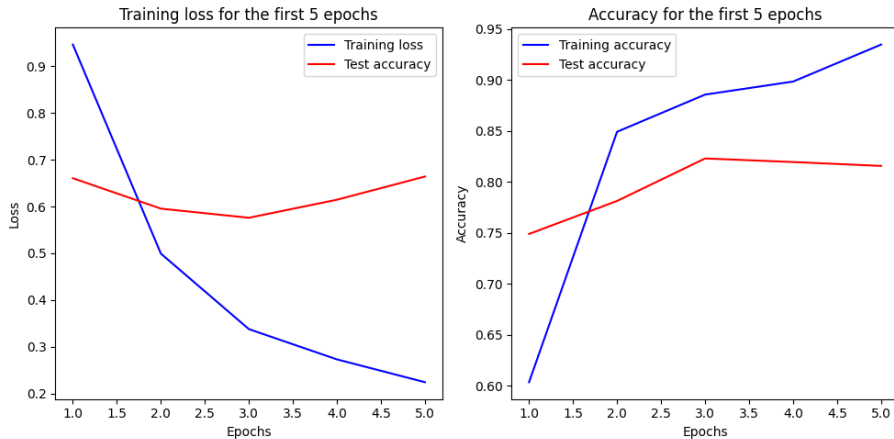


Figure 15: Aztec-CNN accuracy and loss graphs for BODMAS (50 features)

We repeat the experiment above using Aztec images generated from 150 features. All parameters are the same for this case as for 50 features case. The loss and accuracy graphs for this experiment are shown in the following Figure 16. It is again clearly visible that the model is significantly overfitting the data. The test accuracy achieved for the CNN on the Aztec image representation based on 150 features is 0.8344.

6.3 Discussion

Tables B.1 and B.2 in Appendix B list the hyperparameters tested (via grid search) for our classic machine learning and CNN experiments, respectively. In these tables, we have also listed the accuracies obtained for each case. Note that the accuracies in these tables are marginally better than the accuracies given in Sections 6.1 and 6.2 above, as here we have considered early stopping.

The accuracies for the various models tested over the two datasets are summarized in the form of a bar graph in Figure 17. Note that for the CNN experiments on the BODMAS dataset, we have used the “150 Features” results from Table B.2, which were better than the “50 Features” results for both the QR and Aztec codes.

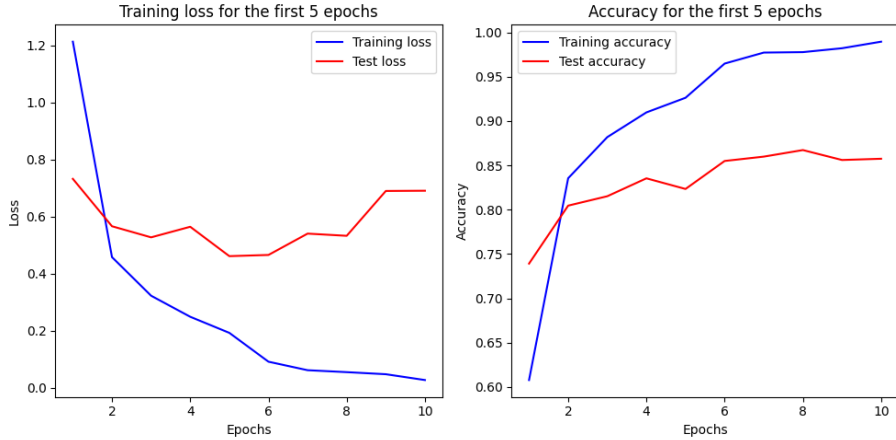


Figure 16: Aztec-CNN accuracy and loss graphs for BODMAS (150 features)

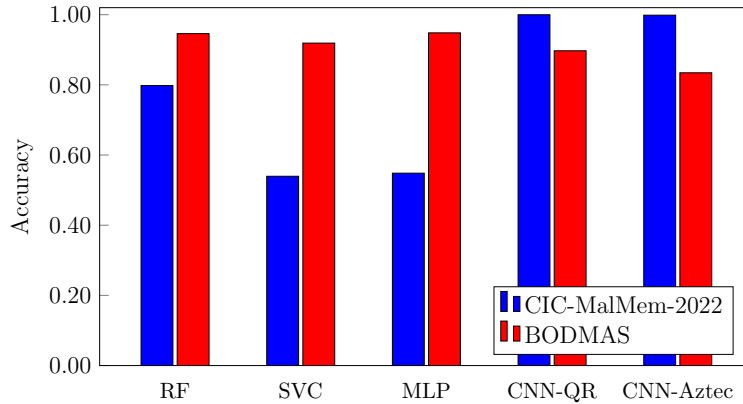


Figure 17: Accuracy comparison graph

From Figure 17, we observe that the QR and Aztec codes far outperform classic techniques on the obfuscated CIC-MalMem-2022 dataset. However, for the BODMAS dataset, the situation is very different, with all three of the classic learning techniques tested outperforming our CNN architectures, regardless of whether the CNN was trained on QR or Aztec codes.

7 Conclusion and Future Work

In recent years, malware detection and classification based on image analysis has received considerable attention in the literature. The method used to construct images from malware can have a major impact on the success of such techniques, yet this aspect of image-based malware analysis has received relatively little attention.

In this paper, we provided an empirical analysis of the utility of QR and

Aztec codes when used to provide image representations of features extracted from malware. We compared CNN models trained on these code images to learning techniques trained directly on the features, using two distinct datasets. Based on these experiments, we found that for the CIC-MalMem-2022 dataset—which consists of dynamic features extracted from obfuscated malware—the QR and Aztec code results were remarkably good. On the other hand, for the more typical malware samples in the BODMAS dataset—which consists of static features—our QR-CNN and Aztec-CNN results did not improve on other, non-image learning approaches. That is, classic ML techniques trained on non-image features performed better on the BODMAS than our more complex QR and Aztec image-based techniques.

There are many possible avenues for future work. Perhaps most urgently, we would like to understand why the QR and Aztec codes perform extremely well on the CIC-MalMem-2022 dataset, yet yielded inferior results on the BODMAS dataset. There are at least three possible reasons for this discrepancy.

- The CIC-MalMem-2022 dataset is derived from obfuscated malware, while BODMAS is not. Perhaps code-based images are superior on more challenging cases, such as obfuscated malware.
- The features in the CIC-MalMem-2022 dataset were determined via dynamic analysis, while the BODMAS features are based on static analysis. It is conceivable that the dynamic features are more informative, and that CNNs trained on code-based images are better able to take advantage of this additional information.
- The CNNs that we trained on the BODMAS dataset showed clear signs of overfitting. Perhaps CNNs would achieve stronger results on this dataset if we reduce this overfitting. Various techniques are available that can often mitigate overfitting in CNNs. For example, cutout regularization [14], which is somewhat analogous to the popular dropout regularization [32] used in other types of neural networks, would be worth testing.

The BODMAS dataset includes accurate timestamps, and hence it is ideal for the study of concept drift [18], which refers to the need to update models when the underlying data has changed. Such “drift” is common in malware, where families evolve as new features are added—existing malware may be adapted for other purposes, new obfuscation techniques may be applied, and so on. If improved results can be obtained for CNNs trained on the BODMAS dataset based on QR or Aztec codes, then testing the robustness of such models under concept drift would be interesting.

Additional tests of QR and Aztec code representations on other malware datasets, as well as other classification problems involving inherently non-image data, would be interesting. Such experiments would enable us to determine the relative strengths and weaknesses of code-based data representations in the realm of machine learning.

References

- [1] Falah Amer Abdulazeez, Ismail Taha Ahmed, and Baraa Tareq Hammad. Examining the performance of various pretrained convolutional neural network models in malware detection. *Applied Sciences*, 14(6), 2024.
- [2] Hyrum S. Anderson and Phil Roth. EMBER: An open dataset for training static PE malware machine learning models. <https://arxiv.org/abs/1804.04637>, 2018.
- [3] John Aycock. *Computer Viruses and Malware*, volume 22 of *Advances in Information Security*. Springer, 2006.
- [4] Aztec code: Barcode guide. https://barcodeguide.seagullscientific.com/content/Symbologies/Aztec_Code.htm, 2024.
- [5] Aztec code generator. <https://pypi.org/project/aztec-code-generator/>, 2023.
- [6] Boaz Barak, Oded Goldreich, Russell Impagliazzo, Steven Rudich, Amit Sahai, Salil Vadhan, and Ke Yang. On the (im)possibility of obfuscating programs. *Journal of the ACM*, 59(2), 2012.
- [7] Ulrich Bayer, Andreas Moser, Christopher Kruegel, and Engin Kirda. Dynamic analysis of malicious code. *Journal in Computer Virology*, 2:67–77, 2006.
- [8] Canadian Institute for Cybersecurity. Malware memory analysis: CIC-MalMem-2022. <https://www.unb.ca/cic/datasets/mallem-2022.html>, 2022.
- [9] Tristan Carrier, Princy Victor, Ali Tekeoglu, and Arash Habibi Lashkari. Detecting obfuscated malware using memory feature engineering. In *The International Conference on Information Systems Security and Privacy*, pages 177–188, 2022.
- [10] Andrew Case and Golden G. Richard. Memory forensics: The path forward. *Digital Investigation*, 20:23–33, 2017.
- [11] Eoghan Casey, editor. *Handbook of Digital Forensics and Investigation*. Elsevier Science, 2009.
- [12] Sibi Chakkaravarthy, Dimple Sangeetha, and V. Vaidehi. A survey on malware analysis and mitigation techniques. *Computer Science Review*, 32:1–23, 2019.
- [13] Murat Dener, Gökçe Ok, and Abdullah Orman. Malware detection using memory analysis data in big data environment. *Applied Sciences*, 12(17):8604, 2022.
- [14] Terrance DeVries and Graham W. Taylor. Improved regularization of convolutional neural networks with cutout. <https://arxiv.org/abs/1708.04552>, 2017.

- [15] Walid El-Shafai, Iman Almomani, and Aala AlKhayer. Visualized malware multi-classification framework using fine-tuned cnn-based transfer learning models. *Applied Sciences*, 11(14), 2021.
- [16] Mahmoud Kalash, Mrigank Rochan, Noman Mohammed, Neil D. B. Bruce, Yang Wang, and Farkhund Iqbal. Malware classification with deep convolutional neural networks. In *2018 9th IFIP International Conference on New Technologies, Mobility and Security*, NTMS, pages 1–5, 2018.
- [17] Maya Hilda Lestari Louk and Bayu Adhi Tama. Tree-based classifier ensembles for PE malware analysis: A performance revisit. *Algorithms*, 15(9), 2022.
- [18] Jie Lu, Anjin Liu, Fan Dong, Feng Gu, João Gama, and Guangquan Zhang. Learning under concept drift: A review. *IEEE Transactions on Knowledge and Data Engineering*, 31(12):2346–2363, 2019.
- [19] Aziz Makandar and Anita Patrot. Malware analysis and classification using artificial neural network. In *2015 International Conference on Trends in Automation, Communications and Computing Technology*, I-TACT-15, pages 1–6, 2015.
- [20] Lakshmanan Nataraj, Shanmugavadivel Karthikeyan, Grégoire Jacob, and B. S. Manjunath. Malware images: visualization and automatic classification. In *Proceedings of the 8th International Symposium on Visualization for Cyber Security*, VizSec '11, 2011.
- [21] NumPy. <https://numpy.org/>, 2023.
- [22] os — miscellaneous operating system interfaces. <https://docs.python.org/3/library/os.html>, 2023.
- [23] Binayak Panda, Sudhanshu Shekhar Bisoyi, and Sidhanta Panigrahy. An ensemble approach for imbalanced multiclass malware classification using 1D-CNN. *PeerJ Computer Science*, 9:e1677, 2023.
- [24] pandas: Powerful python data analysis toolkit. <https://pandas.pydata.org/>, 2023.
- [25] Pillow: The friendly PIL fork. <https://python-pillow.org/>, 2023.
- [26] Pratikkumar Prajapati and Mark Stamp. An empirical analysis of image-based learning techniques for malware classification. In Mark Stamp, Mamoun Alazab, and Andrii Shalaginov, editors, *Malware Analysis Using Artificial Intelligence and Deep Learning*, pages 411–435. Springer, 2021.
- [27] Python QR code. <https://pypi.org/project/qrcode/>, 2023.
- [28] QR code standardization. <https://www.qrcode.com/en/about/standards.html>, 2024.
- [29] Manikandan Ravikiran and Krishna Madgula. Fusing deep quick response code representations improves malware text classification. In *Proceedings of the ACM Workshop on Crossmodal Learning and Application*, WCRML '19, pages 11–18, 2019.

- [30] Scikit-learn: Machine learning in Python. <https://scikit-learn.org/stable/>, 2023.
- [31] Asaf Shabtai, Robert Moskovitch, Yuval Elovici, and Chanan Glezer. Detection of malicious code by applying machine learning classifiers on static features: A state-of-the-art survey. *Information Security Technical Report*, 14(1):16–29, 2009.
- [32] Nitish Srivastava, Geoffrey Hinton, Alex Krizhevsky, Ilya Sutskever, and Ruslan Salakhutdinov. Dropout: A simple way to prevent neural networks from overfitting. *Journal of Machine Learning Research*, 15(1):1929–1958, 2014.
- [33] Mark Stamp. A survey of machine learning algorithms and their application in information security. In Simon Parkinson, Andrew Crampton, and Richard Hill, editors, *Guide to Vulnerability Analysis for Computer Networks and Systems — An Artificial Intelligence Approach*, Computer Communications and Networks, pages 33–55. Springer, 2018.
- [34] Mark Stamp. *Introduction to Machine Learning with Applications in Information Security*. Chapman and Hall/CRC, 2nd edition, 2022.
- [35] TensorFlow. <https://www.tensorflow.org/>, 2023.
- [36] Min-Jen Tsai, Ya-Chu Lee, and Te-Ming Chen. Implementing deep convolutional neural networks for QR code-based printed source identification. *Algorithms*, 16(3), 2023.
- [37] Limin Yang, Arridhana Ciptadi, Ihar Laziuk, Ali Ahmadzadeh, and Gang Wang. BODMAS: An open dataset for learning based temporal analysis of PE malware. In *2021 IEEE Security and Privacy Workshops, SPW*, pages 78–84, 2021.
- [38] Ilsun You and Kangbin Yim. Malware obfuscation techniques: A brief survey. In *2010 International Conference on Broadband, Wireless Computing, Communication and Applications*, pages 297–300, 2010.

Appendix A

In Table A.1, we provide a complete list of the 55 features that appear in the CIC-MalMem-2022 dataset. These features form the basis of experiments discussed in Section 6.1 of this paper, and the top 10 most informative of these 55 features are listed in Table 2,

Recall that the features listed in Table A.1 are derived from memory dumps of selected malware samples. For additional information on these features, see [8].

Table A.1: List of features for CIC-MalMem-2022 dataset

Index	Feature	Index	Feature
1	pslist.nproc	29	malfind.protection
2	pslist.nppid	30	malfind.uniqueInjections
3	pslist.avg_threads	31	psxview.not_in_pslist
4	pslist.nprocs64bit	32	psxview.not_in_eprocess_pool
5	pslist.avg_handlers	33	psxview.not_in_ethread_pool
6	dlllist.ndlls	34	psxview.not_in_pspcid_list
7	dlllist.avg_dlls_per_proc	35	psxview.not_in_csrss_handles
8	handles.nhandles	36	psxview.not_in_session
9	handles.avg_handles_per_proc	37	psxview.not_in_deskthrd
10	handles.nport	38	psxview.not_in_pslist_false_avg
11	handles.nfile	39	psxview.not_in_eprocess_pool_false_avg
12	handles.nevent	40	psxview.not_in_ethread_pool_false_avg
13	handles.ndesktop	41	psxview.not_in_pspcid_list_false_avg
14	handles.nkey	42	psxview.not_in_csrss_handles_false_avg
15	handles.nthread	43	psxview.not_in_session_false_avg
16	handles.ndirectory	44	psxview.not_in_deskthrd_false_avg
17	handles.nsemaphore	45	modules.nmodules
18	handles.ntimer	46	svcsan.nservices
19	handles.nsection	47	svcsan.kernel_drivers
20	handles.nmutant	48	svcsan.fs_drivers
21	ldrmodules.not_in_load	49	svcsan.process_services
22	ldrmodules.not_in_init	50	svcsan.shared_process_services
23	ldrmodules.not_in_mem	51	svcsan.interactive_process_services
24	ldrmodules.not_in_load_avg	52	svcsan.nactive
25	ldrmodules.not_in_init_avg	53	callbacks.ncallbacks
26	ldrmodules.not_in_mem_avg	54	callbacks.nanonymous
27	malfind.ninjections	55	callbacks.ngeneric
28	malfind.commitCharge	—	—

Appendix B

In Tables B.1 and B.2 we list the hyperparameters tested (via grid search) for the classic techniques and our CNN models, respectively. Note that for each model, the selected values are given in boldface.

Table B.1: Hyperparameters tested for classic techniques (selected values in boldface)

Dataset	Classifier	Hyperparameters	Tested values	Accuracy
CIC-MalMem-2022	RF	<code>n_estimators</code> <code>criterion</code> Number of features	[100, 500, 1000] [gini , entropy] [10 , 55]	0.7980
CIC-MalMem-2022	SVC	<code>kernel</code> <code>gamma</code> Number of features	[rbf , poly] [auto, scale] [50 , 150]	0.5395
CIC-MalMem-2022	MLP	<code>hidden_layer_sizes</code> <code>solver</code> <code>max_iter</code> Number of features	[(10,10,10), (15, 10, 10)] [sgd, Adam] [50, 100, 200] [10, 55]	0.5483
BODMAS	RF	<code>n_estimators</code> <code>criterion</code> Number of features	[100, 500, 1000] [gini , entropy] [50 , 150]	0.9460
BODMAS	SVC	<code>kernel</code> <code>gamma</code> Number of features	[rbf , poly] [auto, scale] [50 , 150]	0.9190
BODMAS	MLP	<code>hidden_layer_sizes</code> <code>solver</code> <code>max_iter</code> Number of features	[(10,10,10), (15, 10, 10)] [sgd, Adam] [50, 100, 200] [50 , 150]	0.9482

Table B.2: Hyperparameters tested for CNNs (selected values in boldface)

Dataset	Code	Hyperparameters	Tested values	Accuracy	
				Train	Test
CIC-MalMem-2022	QR	learning_rate	[0.001 , 0.0001]	0.9996	0.9998
		batch_size	[32, 64 , 128]		
		Epochs	[5 , 10, 20]		
		Optimizer	[Adam , RMSProp]		
		image_dim	[128 , 175]		
CIC-MalMem-2022	Aztec	learning_rate	[0.001 , 0.0001]	0.9998	0.9986
		batch_size	[32, 64 , 128]		
		Epochs	[5 , 10, 20]		
		Optimizer	[Adam , RMSProp]		
		image_dim	[128 , 175]		
BODMAS (50 Features)	QR	learning_rate	[0.001 , 0.0001]	0.9386	0.8271
		batch_size	[32, 64 , 128]		
		Epochs	[5 , 10, 20]		
		Optimizer	[Adam , RMSProp]		
		image_dim	[128 , 256]		
BODMAS (50 Features)	Aztec	learning_rate	[0.001 , 0.0001]	0.9288	0.7821
		batch_size	[32, 64 , 128]		
		Epochs	[5 , 10, 20]		
		Optimizer	[Adam , RMSProp]		
		image_dim	[128 , 256, 375]		
BODMAS (150 Features)	QR	learning_rate	[0.001 , 0.0001]	0.9762	0.8971
		batch_size	[32, 64 , 128]		
		Epochs	[5 , 10, 20]		
		image_dim	[128, 256 , 512, 675]		
BODMAS (150 Features)	Aztec	learning_rate	[0.001 , 0.0001]	0.9521	0.8344
		batch_size	[32, 64 , 128]		
		Epochs	[5 , 10, 20]		
		Optimizer	[NAdam , Adam]		
		image_dim	[128, 256 , 512, 675]		